Wirelessly Powered Cell-Free IoT: Analysis and Optimization

Xinhua Wang[®], Member, IEEE, Alexei Ashikhmin[®], Fellow, IEEE, and Xiaodong Wang[®], Fellow, IEEE

Abstract—In this article, we propose a wirelessly powered Internet-of-Things (IoT) system based on the cell-free massive MIMO technology. In such a system, during the downlink phase, the sensors harvest radio-frequency (RF) energy emitted by the distributed access points (APs). During the uplink phase, sensors transmit data to the APs using the harvested energy. Collocated massive MIMO and small-cell IoT can be treated as special cases of cell-free IoT. We derive the tight closed-form lower bound on the amount of harvested energy, and the closed-form expression of SINR as the metrics of power transfer and data transmission, respectively. To improve energy efficiency, we jointly optimize the uplink and downlink power control coefficients to minimize the total transmit energy consumption while meeting the target SINRs. Extended simulation results show that cell-free IoT outperforms collocated massive MIMO and small-cell IoT in terms of both downlink and uplink 95% likely performances. Moreover, significant gains can be achieved by the proposed joint power control in terms of both per user throughput and energy consumption.

Index Terms—Cell-free massive MIMO, Internet of Things (IoT), power control, wireless power transfer (WPT).

I. INTRODUCTION

THE Internet of Things (IoT) is envisioned as a promising technology which enables massively connected intelligent devices to share information and to coordinate decisions [1], [2]. The concept of IoT has brought revolutionary applications in a wild range of domains, including transportation, smart healthcare, environmental monitoring, smart home, and so on. However, the short battery life of the devices causes a bottleneck hampering the proliferation of IoT [3].

Wireless power transfer (WPT) has recently gained significant attention since it allows to prolong the lifetime of IoT and it is more controllable and reliable compared with ambient sources, such as solar, wind, etc. [4], [5]. In wirelessly powered communication networks (WPCNs), the terminals first harvest

Manuscript received October 10, 2019; revised February 17, 2020, March 27, 2020, and April 19, 2020; accepted April 20, 2020. Date of publication April 27, 2020; date of current version September 15, 2020. This work was supported in part by the Natural Science Foundation of Shandong under Grant ZR2017MF066, in part by the U.S. National Science Foundation under Grant CCF1814803, and in part by the National Natural Science Foundation of China under Grant 61561046 and Grant 61761008. (Corresponding author: Xinhua Wang.)

Xinhua Wang is with the College of Electrical Engineering, Qingdao University, Qingdao 266071, China (e-mail: xhwang@qdu.edu.cn).

Alexei Ashikhmin is with the Communications and Statistical Sciences Research Department, Nokia Bell Labs, Murray Hill, NJ 07974 USA (e-mail: alexei.ashikhmin@nokia-bell-labs.com).

Xiaodong Wang is with the Electrical Engineering Department, Columbia University, New York, NY 10027 USA (e-mail: wangx@ee.columbia.edu). Digital Object Identifier 10.1109/JIOT.2020.2990378

radio-frequency (RF) energy from the WPT beacons and then transmit information in the following time slots [6], [7]. This approach can be extended to IoT networks with a large number of low-power sensors. To maximize the system throughput, Chu *et al.* [3] jointly optimized the energy beamforming vector and time allocation duration for a wirelessly powered IoT network.

The main challenge of WPT is the low efficiency due to radio scattering and path loss [8], [9]. As effective countermeasures, MIMO, and especially massive MIMO techniques, have been adopted in WPCNs [10], so that the sensors can harvest more energy since the RF energy becomes more concentrated. For massive MIMO-based WPCN, Wu et al. [11] investigated the asymptotically optimal downlink power allocation strategy to maximize the uplink sum rate. The massive MIMOpowered two-way and multiway relay networks were investigated in [12] and [13], respectively. However, the performance of cell-boundary terminals is still poor due to the heavy path loss. The distributed antenna system (DAS) is adopted to reduce the path loss and improve the WPT efficiency. For the distributed WPT system, Lee and Zhang [14] studied the effective channel training method for optimal energy beamforming with and without coordination. Kim and Yoon [15] proposed a joint time allocation and energy beamforming approach to maximize the energy efficiency of WPCN with distributed antennas. To maximize the average worst case SINR under energy harvesting constraints, Zhu et al. [16] jointly optimized the beamforming vectors and the power splitting factors for a multiuser DAS.

Recently, cell-free massive MIMO wireless systems attracted intensive research interests. In cell-free massive MIMO, a large number of access points (APs) are distributed over a large area. These APs collaboratively serve a large number of terminals using the same time-frequency resource [17], [18]. In contrast to collocated (cellular) massive MIMO, cell-free massive MIMO is a user-centric architecture [19], since each terminal is served by the adjacent distributed APs. Compared with collocated massive MIMO, cell-free massive MIMO typically yields a high degree of macro-diversity and low path loss, since the service antennas are close to the sensors. Ngo et al. [20] derived the closedform expressions of spectral efficiency and energy efficiency for the downlink cell-free massive MIMO system. To improve the spectral efficiency or energy efficiency, the precoding and power control are investigated in [18] and [21]. In a word, the cell-free massive MIMO can reap all benefits from DAS and massive MIMO. Recently, first results on cell-free IoT

2327-4662 © 2020 IEEE. Personal use is permitted, but republication/redistribution requires IEEE permission. See https://www.ieee.org/publications/rights/index.html for more information.

(IoT based on cell-free massive MIMO) have been obtained in [22].

Motivation and Contribution: It is intuitively clear that in cell-free IoT systems, the sensors can harvest more energy during the downlink power transfer phase and reduce the power consumption during the uplink data transmission phase. Motivated by such double-fold benefits, we consider a cell-free massive MIMO based IoT, in which some active sensors transmit signals to APs using the harvested energy during the downlink WPT. Our proposed framework can be widely applied in wireless sensor networks with energy-limited devices, such as the IoT networks for monitoring the environment pollution, the health conditions of patients, and so on.

Our contributions in this article are twofold.

- 1) We propose the framework of wireless-powered IoT based on cell-free massive MIMO. Collocated massive MIMO and small-cell IoT can be treated as special cases of cell-free IoT. We derive the tight closed-form lower bound on the amount of harvested energy, and the closed-form expression of SINR for three systems (cell-free IoT, collocated massive MIMO, and small-cell IoT), respectively. Numerical comparisons show that the cell-free IoT system has the best uplink and downlink 95% likely performances.
- 2) The uplink and downlink power control coefficients are jointly optimized to minimize the total energy consumption while meeting the predefined target SINR. The problem is equivalently decomposed into a linear optimization problem for uplink data transmission, and a quadratic optimization problem for downlink power transfer. Closed-form solutions to both problems are provided.

Different from the previous works on WPCNs, we propose the wirelessly powered cell-free IoT with the user-centric architecture and nonorthogonal random pilots. Due to the nonorthogonal pilots, the estimates of channel vectors between different sensors and the same AP are dependent, which leads to challenges for deriving the closed-form expressions of the amount of harvested energy for WPT and SINR for data transmission.

The remainder of this article is organized as follows. In Section II, we describe the system model and outline our results. In Section III, we derive expressions for uplink and downlink performances. In Section IV, we formulate and solve the joint power control problem. The simulation results are given in Section V. Finally, Section VI concludes this article.

Notation: Throughout this article, scalars and vectors are denoted by lowercase letters and boldface lowercase letters, respectively. Diag(a) denotes a diagonal matrix with diagonal entries are equal to the components of a. $|\cdot|$ and $||\cdot||$ represent the absolute value and the ℓ_2 norm, respectively. $(\cdot)^H$ and $(\cdot)^{-1}$ denote the conjugate transpose and the inverse operation, respectively. [A]_{mm} returns the mth diagonal element of A. $\mathcal{CN}(\mathbf{m}, \mathbf{R})$ denotes the circularly symmetric complex Gaussian (CSCG) distribution with mean \mathbf{m} and covariance matrix \mathbf{R} . $\mathbb{E}[\cdot]$ and $\text{var}\{\cdot\}$ stand for the expectation and variance operations, respectively.

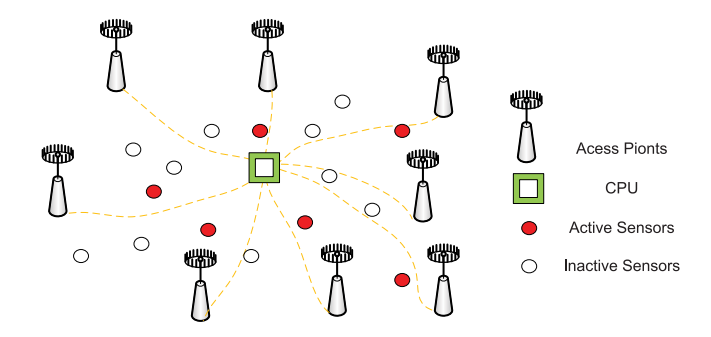


Fig. 1. Cell-free massive MIMO with distributed APs serving active sensors.

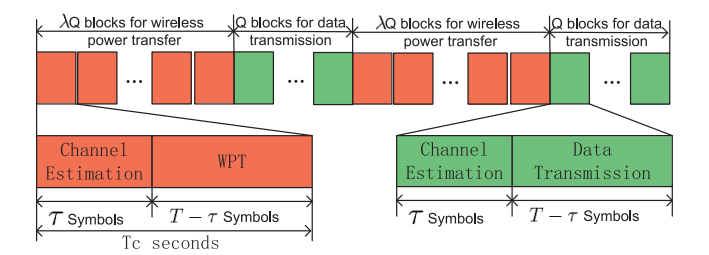


Fig. 2. Frame structure.

II. SYSTEM MODEL AND OUTLINE OF RESULTS

As shown in Fig. 1, L distributed APs and a large number of sensors are randomly located in an area. Among them, there are K active sensors indexed as $1, \ldots, K$ in a given period. We consider a wirelessly powered IoT based on cell-free massive MIMO which can be deemed as a sufficient large network wrapped around by this area. All APs connect to a central processing unit (CPU) via a perfect backhaul network, which implies that there is no handover when a user moves. Different from DAS, the cell-free IoT is user centric, that is, each sensor is served by the closest L APs. Each AP is equipped with N antennas and each user has a single antenna. The channel coefficient between the kth sensor and the nth antenna of the kth AP is denoted as

$$g_{(l,n),k} = \sqrt{\beta_{l,k}} h_{(l,n),k}$$

where $\beta_{l,k}$ represents the large-scale fading and is assumed known, and $h_{(l,n),k} \sim \mathcal{CN}(0,1)$ is the small-scale fading. Denote $\mathbf{g}_{(l,n)}$ as the channel vector between the nth antenna of the lth AP and active sensors, and $\mathbf{g}_{l,j}$ as the channel vector between the lth AP and the jth sensor, i.e.,

$$\mathbf{g}_{(l,n)} = \left[g_{(l,n),1}, \dots, g_{(l,n),K}\right]^{\mathrm{T}} \in \mathbb{C}^{K \times 1}$$

and

$$\mathbf{g}_{l,j} = \left[g_{(l,1),j}, \dots, g_{(l,N),j} \right]^{\mathrm{T}} \in \mathbb{C}^{N \times 1}.$$

As shown in Fig. 2, we partition communication into periods, and each period includes $(\lambda+1)Q$ consecutive coherence time blocks. In each period, the K active users first harvest RF energy emitted by APs over λQ time blocks, and next transmit data to APs in the remaining time blocks using the harvested energy. Each coherence time T_c block contains T OFDM symbols, in which τ symbols are used for channel estimation, while the remaining symbols are used for WPT or data transmission.

A. System Model

1) Downlink WPT: During the τ symbols in each time slot, all K active sensors simultaneously transmit their pilot sequences to all APs for channel estimation. Let $\psi_k \in \mathbb{C}^{\tau}$ with $\|\psi_k\|^2 = 1$ be the pilot sequence of the kth sensor. Denote $\Psi = [\psi_1, \dots, \psi_K] \in \mathbb{C}^{\tau \times K}$, the received pilots $y_{(l,n)} \in \mathbb{C}^{\tau}$ at the nth antenna of the lth AP are given by

$$\mathbf{y}_{(l,n)} = \sqrt{\tau \rho_p} \sum_{k=1}^{K} g_{(l,n),k} \boldsymbol{\varphi}_k + \boldsymbol{w}_{(l,n)}$$
$$= \sqrt{\tau \rho_p} \boldsymbol{\Psi} \boldsymbol{g}_{(l,n)} + \boldsymbol{w}_{(l,n)}$$
(1)

where $\mathbf{w}_{(l,n)} \sim \mathcal{CN}(0,\mathbf{I})$ is the additive noise, and ρ_p is the normalized pilot transmit power. Given $\mathbf{y}_{(l,n)}$, the channel estimate $\hat{\mathbf{g}}_{(l,n)}$ is obtained by using the linear minimum mean-square-error (LMMSE) method.

During the remaining symbols in each time slot, the APs use the estimated channels to conduct conjugate beamforming and simultaneously transmit signals to all sensors. Denote by $\eta_{l,j}$ the power control coefficients of the *l*th AP for the *j*th sensor, and by $q_j \sim \mathcal{CN}(0,1)$ the symbol intended for this sensor. The received signal at the *k*th sensor is

$$z_k = \sum_{l=1}^{L} \mathbf{g}_{l,k}^{\mathrm{T}} \mathbf{x}_l + v_k \tag{2}$$

where $v_k \sim \mathcal{CN}(0, 1)$ is the additive noise at the kth sensor, and $\mathbf{x}_l = \sqrt{\rho_d} \sum_{j=1}^K \sqrt{\eta_{l,j}} \hat{\mathbf{g}}_{l,j}^* q_j$ is the transmitted signal from the lth AP with

$$\Xi_l = \mathbb{E} \Big[\| \mathbf{x}_l \|^2 \Big] \le N \rho_d \tag{3}$$

where $N\rho_d$ is the maximum transmit power of each AP. Thus, the total energy consumption during the λQ downlink WPT time blocks is

$$\Xi_{\rm tr} = \left(1 - \frac{\tau}{T}\right) \lambda Q \sum_{l=1}^{L} \Xi_l \tag{4}$$

while the harvested energy of the kth sensor during the λQ WPT time blocks can be expressed as

$$\mathcal{E}_{k} = \left(1 - \frac{\tau}{T}\right) \lambda Q \zeta \mathbb{E}\left[|z_{k}|^{2}\right]$$
 (5)

where $\zeta \in [0, 1]$ is the energy conversion efficiency.

2) Uplink Data Transmission: During the τ symbols in each time slot, channel estimation is performed in the same way as the downlink WPT case. During the remaining symbols in each time slot, K users simultaneously transmit their data to all APs. Let ρ_u be the maximum normalized transmit power of each sensor. Let $\xi_j \in [0, 1]$ be the power control coefficient, and s_j be the data symbol of the jth user with $\mathbb{E}[|s_j|^2] = 1$. Then, the received signal $r_l \in \mathbb{C}^N$ at the lth AP is

$$\mathbf{r}_{l} = \sqrt{\rho_{u}} \sum_{j=1}^{K} \sqrt{\xi_{j}} \mathbf{g}_{l,j} s_{j} + \mathbf{n}_{l}$$
 (6)

where $n_l \sim \mathcal{CN}(\mathbf{0}, I_N)$ is the additive noise. To detect symbol s_k , the lth AP computes $\hat{\mathbf{g}}_{l,k}^H \mathbf{r}_l$ and sends it to the CPU. The

CPU employs the equal gain combining (EGC) to detect s_k as follows:

$$\hat{s}_{k} = \sum_{l=1}^{L} \hat{\mathbf{g}}_{l,k}^{H} \mathbf{r}_{l}$$

$$= \sqrt{\rho_{u} \xi_{k}} \sum_{l=1}^{L} \mathbb{E} \left[\hat{\mathbf{g}}_{l,k}^{H} \mathbf{g}_{l,k} \right] s_{k}$$

$$+ \sqrt{\rho_{u} \xi_{k}} \sum_{l=1}^{L} \left(\hat{\mathbf{g}}_{l,k}^{H} \mathbf{g}_{l,k} - \mathbb{E} \left[\hat{\mathbf{g}}_{l,k}^{H} \mathbf{g}_{l,k} \right] \right) s_{k}$$

$$+ \sum_{j \neq k}^{K} \sqrt{\rho_{u} \xi_{j}} \sum_{l=1}^{L} \hat{\mathbf{g}}_{l,k}^{H} \mathbf{g}_{l,j} s_{j} + \sum_{l=1}^{L} \hat{\mathbf{g}}_{l,k}^{H} \mathbf{n}_{l}$$

$$+ \sum_{j \neq k}^{K} \sqrt{\rho_{u} \xi_{j}} \sum_{l=1}^{L} \hat{\mathbf{g}}_{l,k}^{H} \mathbf{g}_{l,j} s_{j} + \sum_{l=1}^{L} \hat{\mathbf{g}}_{l,k}^{H} \mathbf{n}_{l}$$

$$(7)$$

where A_1 is the desired signal, and A_2 , A_3 , and A_4 are the beamforming uncertainty, interuser interference due to the nonorthogonality of the pilots, and noise, respectively. It is not difficult to show that A_1 , A_2 , A_3 , and A_4 are uncorrelated. Hence, according to [23], the worst case is the AWGN channel with the effective noise $A_2 + A_3 + A_4$. Thus, similar as in [17], the capacity of the kth sensor is lower bounded by

$$C_k = \log_2(1 + \Gamma_k) \text{ b/s/Hz}$$
 (8)

with the effective SINR

$$\Gamma_k = \frac{|\mathcal{A}_1|^2}{\mathbb{E}[|\mathcal{A}_2|^2] + \mathbb{E}[|\mathcal{A}_3|^2] + \mathbb{E}[|\mathcal{A}_4|^2]}$$
(9)

where the expectation is with respect to the small-scale fading. In addition, the energy consumption of the kth sensor during successive Q time blocks for data transmission is

$$E_k(\xi_k) = \left(1 - \frac{\tau}{T}\right) Q \rho_u \xi_k. \tag{10}$$

B. Outline of Results

To evaluate the performance of the cell-free IoT, a collocated massive MIMO system and a small-cell system are also considered as benchmarks for comparison. The collocated massive MIMO can be treated as a special case of cell-free IoT, where all L APs are collocated, which implies $\beta_{l,k} = \beta_k \ \forall l$. For the small-cell system, we assume that user k is served by only one AP that has the largest $\beta_{l,k}$ coefficient. We define the following binary association coefficient:

$$\delta_{l,j} = \begin{cases} 1, & \text{jth sensor is associated with the } l \text{th AP} \\ 0, & \text{otherwise.} \end{cases}$$

Then, the received signal at the *k*th sensor during the downlink WPT phase [corresponding to (2) of cell-free IoT] is

$$z_k^{\text{sc}} = \sum_{l=1}^{L} \delta_{l,k} \boldsymbol{g}_{l,k}^{\text{T}} \boldsymbol{x}_l^{\text{sc}} + v_k$$

where $\mathbf{x}_{l}^{sc} = \sqrt{\rho_{d}} \sum_{j=1}^{K} \sqrt{\delta_{l,j} \eta_{l,j}} \hat{\mathbf{g}}_{l,j}^{*} q_{j}$ is the transmitted signal at the *l*th AP. Similar as cell-free IoT, during uplink data

transmission, the estimate of s_k is

$$\hat{s}_k^{\text{sc}} = \sum_{l=1}^L \delta_{l,k} \hat{\boldsymbol{g}}_{l,k}^H \boldsymbol{r}_l.$$

Hence, the small-cell system can also be treated as a special case of cell-free IoT with $\hat{\mathbf{g}}_{l,k} = \delta_{l,k}\hat{\mathbf{g}}_{l,k}$.

In Section III, we derive the tight closed-form lower bound of \mathcal{E}_k in (5) and the closed-form expression of Γ_k in (9) as the metrics of WPT and data transmission, respectively, for the three systems. The numerical results reveal that cell-free massive MIMO achieves higher \mathcal{E}_k and Γ_k given the same power control coefficients. This is because, compared with collocated massive MIMO, the cell-free massive MIMO can achieve more macrodiversity since the sensors are closer to APs; and compared with small cells, the cooperation between different APs leads to higher array gain.

Then, in Section IV, we jointly optimize the downlink and uplink power control coefficients η and ξ , and the WPT duration λ to further improve the efficiency of the cell-free IoT. We aim to minimize the energy consumption of APs Ξ_{tr} in (4) while meeting a given target SINR during data transmission supported by the harvested energy.

III. PERFORMANCE ANALYSIS

In this section, we derive tight closed-form lower bounds on \mathcal{E}_k in (5), and the closed-form expressions of Γ_k in (9) for cell-free massive MIMO, collocated massive MIMO, and small-cell systems.

A. LMMSE Channel Estimation

According to (1), we have

$$\mathbb{E}\left[\mathbf{y}_{(l,n)}\mathbf{y}_{(l,n)}^{H}\right] = \mathbb{E}\left[\left(\sqrt{\tau\rho_{p}}\mathbf{\Psi}\mathbf{g}_{(l,n)} + \mathbf{w}_{(l,n)}\right) \times \left(\sqrt{\tau\rho_{p}}\mathbf{g}_{(l,n)}^{H}\mathbf{\Psi}^{H} + \mathbf{w}_{(l,n)}^{H}\right)\right]$$
$$= \tau\rho_{n}\mathbf{\Psi}\mathbf{D}_{l}\mathbf{\Psi}^{H} + \mathbf{I}$$

and

$$\mathbb{E}\left[\boldsymbol{g}_{(l,n)}\boldsymbol{y}_{(l,n)}^{H}\right] = \mathbb{E}\left[\boldsymbol{g}_{(l,n)}\left(\sqrt{\tau\rho_{p}}\boldsymbol{g}_{(l,n)}^{H}\boldsymbol{\Psi}^{H} + \boldsymbol{w}_{(l,n)}^{H}\right)\right]$$

$$= \mathbb{E}\left[\sqrt{\tau\rho_{p}}\boldsymbol{g}_{(l,n)}\boldsymbol{g}_{(l,n)}^{H}\boldsymbol{\Psi}^{H} + \boldsymbol{g}_{(l,n)}\boldsymbol{w}_{(l,n)}^{H}\right]$$

$$= \sqrt{\tau\rho_{p}}\boldsymbol{D}_{l}\boldsymbol{\Psi}^{H}$$

where $D_l = \mathbb{E}[\mathbf{g}_{(l,n)}\mathbf{g}_{(l,n)}^H] = \operatorname{diag}(\beta_{l,1},\ldots,\beta_{l,k})$. Thus, the LMMSE channel estimate of $\mathbf{g}_{(l,n)}$ is

$$\hat{\boldsymbol{g}}_{(l,n)} = \mathbb{E} \Big[\boldsymbol{g}_{(l,n)} \boldsymbol{y}_{(l,n)}^H \Big] \Big(\mathbb{E} \Big[\boldsymbol{y}_{(l,n)} \boldsymbol{y}_{(l,n)}^H \Big] \Big)^{-1} \boldsymbol{y}_{(l,n)}$$

$$= \sqrt{\tau \rho_p} \boldsymbol{D}_l \boldsymbol{\Psi}^H \Big(\tau \rho_p \boldsymbol{\Psi} \boldsymbol{D}_l \boldsymbol{\Psi}^H + \boldsymbol{I} \Big)^{-1} \boldsymbol{y}_{(l,n)}$$

$$= \boldsymbol{A}_l^H \boldsymbol{y}_{(l,n)}$$
(11)

where

$$oldsymbol{A}_l = \sqrt{ au
ho_p} ig(au
ho_p oldsymbol{\Psi} oldsymbol{D}_l oldsymbol{\Psi}^H + oldsymbol{I}ig)^{-1} oldsymbol{\Psi} oldsymbol{D}_l.$$

Thus, we have

$$\mathbb{E}\left[\hat{\boldsymbol{g}}_{(l,n)}\hat{\boldsymbol{g}}_{(l,n)}^{H}\right] = \sqrt{\tau\rho_{p}}\boldsymbol{D}_{l}\boldsymbol{\Psi}^{H}\boldsymbol{A}_{l}.$$
(12)

The estimated channel $\hat{g}_{(l,n)}$ includes K Gaussian distributed variables with

$$\gamma_{l,k} = \mathbb{E}\Big[\big|\hat{g}_{(l,n),k}\big|^2\Big] = \Big[\mathbb{E}\Big(\hat{g}_{(l,n)}\hat{g}_{(l,n)}^H\Big)\Big]_{kk} \\
= \sqrt{\tau \rho_p} \beta_{l,k} \boldsymbol{\psi}_k^H \boldsymbol{a}_{l,k} = \tau \rho_p \beta_{l,k}^2 \boldsymbol{\psi}_k^H \boldsymbol{Z}_l^{-1} \boldsymbol{\psi}_k \tag{13}$$

where

$$\mathbf{Z}_{l} = \tau \rho_{p} \mathbf{\Psi} \mathbf{D}_{l} \mathbf{\Psi}^{H} + \mathbf{I} \tag{14}$$

and

$$\boldsymbol{a}_{l,k} = \sqrt{\tau \rho_p} \beta_{l,k} \mathbf{Z}_l^{-1} \boldsymbol{\psi}_k \tag{15}$$

is the kth column of A_l . It is also useful to write explicitly that

$$\hat{g}_{(l,n),k} = \boldsymbol{a}_{l,k}^{H} \left(\sqrt{\tau \rho_{p}} \sum_{i=1}^{K} g_{(l,n),i} \boldsymbol{\varphi}_{i} + \boldsymbol{w}_{(l,n)} \right).$$
 (16)

From (16), the channel estimate $\hat{g}_{(l,n),k}$ depends on all the channel coefficients $\{g_{(l,n),i}, i=1,\ldots,K\}$ which is due to the nonorthogonal random pilots. Hence, the estimates of channel vectors between different sensors and the same AP are dependent, i.e.,

$$\operatorname{cov}[\hat{\boldsymbol{g}}_{l,k},\hat{\boldsymbol{g}}_{l,i}] \neq \boldsymbol{0}, \quad k, i = 1, \dots, K.$$

The dependence between $\hat{\mathbf{g}}_{l,k}$ and $\hat{\mathbf{g}}_{l,i}$ leads to challenges for deriving the closed-form expressions of \mathcal{E}_k in (5) and Γ_k in (9). To derive the closed-form expressions of \mathcal{E}_k and Γ_k , we first introduce the following lemma.

Lemma 1: The estimates of channel vectors between different APs and the same sensor are uncorrelated, i.e.,

$$\operatorname{cov}[\hat{\mathbf{g}}_{l,k}, \hat{\mathbf{g}}_{m,k}] = \mathbf{0}, \quad m, l \in \{1, \dots, L\}, \quad m \neq l$$

 $k = 1, \dots, K.$

Moreover, the corresponding norms are also uncorrelated, i.e.,

$$\operatorname{cov}\left[\left\|\hat{\boldsymbol{g}}_{l,k}\right\|^{2},\left\|\hat{\boldsymbol{g}}_{m,k}\right\|^{2}\right]=0.$$

Proof: See Appendix A.

B. Results for Cell-Free IoT

1) Downlink Power Transfer: Let $\tilde{\mathbf{g}}_{l,k} = \mathbf{g}_{l,k} - \hat{\mathbf{g}}_{l,k}$ be the channel estimation error. The received signal at the kth user in (2) can be rewritten as

$$z_k = S_{k1} + S_{k2} + S_{k3} \tag{17}$$

where

$$\mathcal{S}_{k1} = \sqrt{\rho_d} \sum_{l=1}^{L} \sqrt{\eta_{l,k}} \hat{\boldsymbol{g}}_{l,k}^{\mathrm{T}} \hat{\boldsymbol{g}}_{l,k}^{*} q_k$$
$$\mathcal{S}_{k2} = \sqrt{\rho_d} \sum_{l=1}^{L} \sqrt{\eta_{l,k}} \tilde{\boldsymbol{g}}_{l,k}^{\mathrm{T}} \hat{\boldsymbol{g}}_{l,k}^{*} q_k$$

and

$$S_{k3} = \sqrt{\rho_d} \sum_{l=1}^{L} \sum_{j \neq k}^{K} \sqrt{\eta_{l,j}} \boldsymbol{g}_{l,k}^{\mathrm{T}} \hat{\boldsymbol{g}}_{l,j}^{*} q_j + v_k.$$

The amount of energy harvested by the kth user during λQ successive time blocks can be expressed as

$$\begin{split} \mathcal{E}_k &= \left(1 - \frac{\tau}{T}\right) \lambda Q \zeta \mathbb{E} \left[|\mathcal{S}_{k1} + \mathcal{S}_{k2} + \mathcal{S}_{k3}|^2 \right] \\ &= \left(1 - \frac{\tau}{T}\right) \lambda Q \zeta \mathbb{E} \left[|\mathcal{S}_{k1}|^2 + |\mathcal{S}_{k2} + \mathcal{S}_{k3}|^2 \right. \\ &+ \left. 2 \Re \left\{ \mathcal{S}_{k1} (\mathcal{S}_{k2} + \mathcal{S}_{k3}) \right\} \right]. \end{split}$$

Note that S_{k1} , S_{k2} , and S_{k3} are uncorrelated since we assume that downlink symbols for different users are uncorrelated. Thus, we have $\mathbb{E}[2\Re\{S_{k1}(S_{k2}+S_{k3})\}]=0$, and this allows us to get the following lower bound for \mathcal{E}_k as shown in (18), at the bottom of the page, where step (a) is obtained according to Lemma 1 and $\tilde{\eta}_{l,k} = \eta_{l,k} \gamma_{l,k}$ should satisfy:

$$\sum_{k=1}^{K} \tilde{\eta}_{l,k} \le 1, \text{ for any AP } l = 1, \dots, L$$

according to (3) and (13), where the constant $\gamma_{l,k}$ is given in (13), which essentially is the estimate of $\beta_{l,k}$.

2) Uplink Data Transmission: Using the method in [22], we get the following closed-form expression of the SINR given in (9), which is a function of the large-scale fading coefficients and the pilot sequences.

Theorem 1: The effective SINR of the kth sensor in cellfree massive MIMO with the LMMSE channel estimation and the EGC receiver is

$$\Gamma_k = \frac{\mathcal{D}_k \xi_k}{\mathcal{U}_k \xi_k + \sum_{j \neq k} \mathcal{I}_{kj} \xi_j + \mathcal{N}_k}$$
(19)

where

$$\mathcal{D}_{k} = \rho_{u} N \left(\sum_{l=1}^{L} \gamma_{l,k} \right)^{2}, \quad \mathcal{U}_{k} = \sum_{l=1}^{L} \rho_{u} \gamma_{l,k} \beta_{l,k}$$

$$\mathcal{N}_{k} = \sum_{l=1}^{L} \gamma_{l,k}$$

and

$$\mathcal{I}_{kj} = \rho_u \sum_{l=1}^{L} \beta_{l,j} \|\boldsymbol{a}_{l,k}\|^2 + \tau \rho_u \rho_p N \left(\sum_{l=1}^{L} \beta_{l,j} \boldsymbol{\psi}_j^H \boldsymbol{a}_{l,k} \right)^2 + \tau \rho_u \rho_p \sum_{l=1}^{L} \sum_{i=1}^{K} \beta_{l,j} \beta_{l,i} (\boldsymbol{\psi}_i^H \boldsymbol{a}_{l,k})^2.$$

Proof: See Appendix B.

Note that Γ_k in (19) depends on not only the uplink power control coefficients $\{\xi_k\}$ but also the random pilots $\{\psi_k\}$. So, the channel estimation plays a more important role than the cases with orthogonal pilots.

C. Results for Collocated Massive MIMO and Small-Cell IoT

The collocated massive MIMO is a special case with $\beta_{l,k} = \beta_k$, $\gamma_{l,k} = \gamma_k$, and $\tilde{\eta}_{l,k} = \tilde{\eta}_k$. So, we have the following corollary.

Corollary 1: For collocated massive MIMO, the amount of energy harvested by the kth user in λQ successive time blocks is lower bounded as

$$\mathcal{E}_k^{\rm cm} \ge \tilde{\mathcal{E}}_k^{\rm cm} = \left(1 - \frac{\tau}{T}\right) \lambda Q \zeta \rho_d L N (L N + 1) \tilde{\eta}_k \gamma_k.$$

The effective SINR of the *k*th sensor during the data transmission phase is given by

$$\Gamma_k^{\text{cm}} = \frac{\mathcal{D}_k^{\text{cm}} \xi_k}{\mathcal{U}_k^{\text{cm}} \xi_k + \sum_{j \neq k} \mathcal{I}_{kj}^{\text{cm}} \xi_j + \mathcal{N}_k^{\text{cm}}}$$

where $\mathcal{D}_k^{\mathrm{cm}} = \rho_u L N(\gamma_k)^2$, $\mathcal{U}_k^{\mathrm{cm}} = \rho_u \gamma_k \beta_k$, $\mathcal{N}_k^{\mathrm{cm}} = \gamma_k$, and $\mathcal{I}_{kj}^{\mathrm{cm}} = \rho_u \beta_j \|\boldsymbol{a}_k\|^2 + \tau \rho_u \rho_p \sum_{i=1}^K \beta_j \beta_i (\boldsymbol{\psi}_i^H \boldsymbol{a}_k)^2 + \tau \rho_u \rho_p L N(\beta_j \boldsymbol{\psi}_j^H \boldsymbol{a}_k)^2$.

Moreover, the small-cell IoT is also a special case with $\hat{\mathbf{g}}_{l,k} = \delta_{l,k}\hat{\mathbf{g}}_{l,k}$ and $\gamma_{l,k} = \delta_{l,k}\gamma_{l,k}$. Substituting them into (18) and (19), we have the following corollary.

Corollary 2: For small-cell IoT, the amount of energy harvested by the kth user in λQ successive time blocks is lower bounded as

$$\mathcal{E}_{k}^{sc} \geq \tilde{\mathcal{E}}_{k}^{sc} = \left(1 - \frac{\tau}{T}\right) \lambda Q \zeta \rho_{d} N(N+1) \sum_{l=1}^{L} \delta_{lk} \tilde{\eta}_{lk} \gamma_{lk}. \tag{20}$$

The effective SINR of the *k*th sensor during the data transmission phase is given by

$$\Gamma_k^{sc} = \frac{\mathcal{D}_k^{sc} \xi_k}{\mathcal{U}_k^{sc} \xi_k + \sum_{j \neq k} \mathcal{I}_{kj}^{sc} \xi_j + \mathcal{N}_k^{sc}}$$

$$\mathcal{E}_{k} \geq \tilde{\mathcal{E}}_{k} = \left(1 - \frac{\tau}{T}\right) \lambda Q \zeta \mathbb{E}\left[|\mathcal{S}_{k1}|^{2}\right] = \left(1 - \frac{\tau}{T}\right) \lambda Q \zeta \rho_{d} \sum_{l=1}^{L} \sum_{m=1}^{L} \mathbb{E}\left[\sqrt{\eta_{l,k}\eta_{m,k}} \hat{\mathbf{g}}_{l,k}^{T} \hat{\mathbf{g}}_{m,k}^{*} \hat{\mathbf{g}}_{m,k}^{*}\right]$$

$$= \left(1 - \frac{\tau}{T}\right) \lambda Q \zeta \rho_{d} \sum_{l=1}^{L} \mathbb{E}\left[\eta_{l,k} \| \hat{\mathbf{g}}_{l,k} \|^{4}\right] + \left(1 - \frac{\tau}{T}\right) \lambda Q \zeta \rho_{d} \sum_{l=1}^{L} \sum_{m \neq l} \mathbb{E}\left[\sqrt{\eta_{l,k}\eta_{m,k}} \| \hat{\mathbf{g}}_{l,k} \|^{2} \| \hat{\mathbf{g}}_{m,k} \|^{2}\right]$$

$$\stackrel{(a)}{=} \left(1 - \frac{\tau}{T}\right) \lambda Q \zeta N(N+1) \rho_{d} \sum_{l=1}^{L} \left(\eta_{l,k} \gamma_{l,k}^{2}\right) + \left(1 - \frac{\tau}{T}\right) \lambda Q \zeta N^{2} \rho_{d} \sum_{l=1}^{L} \sum_{m \neq l} \left(\sqrt{\eta_{l,k}\eta_{m,k}} \gamma_{l,k} \gamma_{m,k}\right)$$

$$= \left(1 - \frac{\tau}{T}\right) \lambda Q \zeta N^{2} \rho_{d} \left(\sum_{l=1}^{L} \sqrt{\eta_{l,k}} \gamma_{l,k}\right)^{2} + \left(1 - \frac{\tau}{T}\right) \lambda Q \zeta N \rho_{d} \sum_{l=1}^{L} \left(\sqrt{\eta_{l,k}\eta_{m,k}} \gamma_{l,k}\right)^{2}$$

$$= \left(1 - \frac{\tau}{T}\right) \lambda Q \zeta N \rho_{d} \left[N \left(\sum_{l=1}^{L} \sqrt{\tilde{\eta}_{l,k}} \gamma_{l,k}\right)^{2} + \sum_{l=1}^{L} \tilde{\eta}_{l,k} \gamma_{l,k}\right]$$

$$(18)$$

where

$$\mathcal{D}_{k}^{sc} = \rho_{u} N \sum_{l=1}^{L} \delta_{l,k} \gamma_{l,k}^{2}, \quad \mathcal{U}_{k}^{sc} = \sum_{l=1}^{L} \rho_{u} \delta_{l,k} \gamma_{l,k} \beta_{l,k}$$
$$\mathcal{N}_{k}^{sc} = \sum_{l=1}^{L} \delta_{l,k} \gamma_{l,k}$$

and

$$\mathcal{I}_{kj}^{sc} = \rho_u \left[\tau \rho_p \sum_{l=1}^{L} \sum_{i=1}^{K} \delta_{l,k} \beta_{l,j} \beta_{l,i} (\boldsymbol{\psi}_i^H \boldsymbol{a}_{l,k})^2 + \sum_{l=1}^{L} \delta_{l,k} \beta_{l,j} \|\boldsymbol{a}_{l,k}\|^2 + \tau \rho_p N \left(\sum_{l=1}^{L} \delta_{l,k} \beta_{l,j} \boldsymbol{\psi}_j^H \boldsymbol{a}_{l,k} \right)^2 \right].$$

IV. JOINT DOWNLINK-UPLINK POWER CONTROL

To improve the energy efficiency of cell-free IoT, we aim to minimize the total energy consumption of APs Ξ_{tr} in (4) while meeting a given target SINR by jointly optimizing the uplink power control coefficients ξ and the downlink energy allocation $\mu = \lambda \tilde{\eta}$ with $\mu_{l,k} = \lambda \tilde{\eta}_{l,k}$. Then, we determine the normalized downlink power control coefficients $\tilde{\eta}$ through minimizing the WPT duration λ . Specifically, the amount of harvested energy in each period of each sensor should satisfy

$$\tilde{\mathcal{E}}_k \ge E_k(\xi_k) + E_0 \quad \forall k$$
 (21)

where $E_k(\xi_k)$ is the energy consumption for data transmission, and E_0 is the energy consumption for the pilot transmission and circuit operation.

Substituting $\mu_{l,k}=\lambda\tilde{\eta}_{l,k}$ into (18), $\tilde{\mathcal{E}}_k$ can be further simplified into

$$\tilde{\mathcal{E}}_{k}(\boldsymbol{\mu}) = \left(1 - \frac{\tau}{T}\right) Q \zeta N \rho_{d} \left[N \left(\sum_{l=1}^{L} \sqrt{\mu_{l,k} \gamma_{l,k}} \right)^{2} + \sum_{l=1}^{L} \mu_{l,k} \gamma_{l,k} \right]. \tag{22}$$

According to (3) and (4) and the definition of x_l , the total energy consumption of APs can be rewritten as

$$\Xi_{\rm tr} = Q \left(1 - \frac{\tau}{T} \right) \rho_d N \sum_{l=1}^{L} \sum_{k=1}^{K} \mu_{l,k}.$$
 (23)

The joint optimization problem is then

P0:
$$\min_{\boldsymbol{\xi}, \boldsymbol{\mu}} \ \Xi_{tr}$$
s.t. $\tilde{\mathcal{E}}_k(\boldsymbol{\mu}) \ge E_k(\boldsymbol{\xi}_k) + E_0 \quad \forall k$

$$\Gamma_k(\boldsymbol{\xi}) \ge \Delta_k \quad \forall k$$
 (24)

$$0 < \xi_k < 1 \quad \forall k \tag{25}$$

$$\mu > 0 \tag{26}$$

where Δ_k is a given target SINR value during the data transmission. Next, we show that **P0** can be equivalently

decomposed into the following two problems:

P1:
$$\min_{\boldsymbol{\xi}} \sum_{k=1}^{K} E_k(\xi_k)$$

s.t. $\Gamma_k(\boldsymbol{\xi}) = \frac{\mathcal{D}_k \xi_k}{\mathcal{U}_{k2} \xi_k + \sum_{j \neq k} \mathcal{I}_{kj} \xi_j + \mathcal{N}_k} \ge \Delta_k \quad \forall k$
 $0 < \xi_k < 1 \quad \forall k$

and

P2:
$$\min_{\boldsymbol{\mu}} \ \Xi_{tr}$$
s.t. $\tilde{\mathcal{E}}_k(\boldsymbol{\mu}) \ge E_k(\xi_k) + E_0 \quad \forall k$

$$\boldsymbol{\mu} > 0. \tag{27}$$

P1 is minimization of the total energy consumption $\sum_{k=1}^{K} E_k(\xi_k)$ subject to the target SINR constraint Δ_k for the uplink data transmission, and **P2** is minimization of the total energy consumption given the target harvested energy constraints for the downlink WPT.

Theorem 2: Solving **P0** is equivalent to solving **P1** and **P2** in sequence.

Proof: From Theorem 3, the optimal solution ξ^* to **P1** is the point that can simultaneously minimize $E_k(\xi_k)$ for all k under the constraints of (24) and (25). That is, for any point $\xi \in \mathbb{P}$ with \mathbb{P} being the feasibility region defined by (24) and (25), we have

$$E_k(\xi_k) \ge E_k(\xi_k^*), \quad k = 1, \dots, K.$$
 (28)

Denote the optimal solution to $\mathbf{P0}$ as $(\boldsymbol{\xi}^{\#}, \boldsymbol{\mu}^{\#})$. It is noted that Ξ_{tr} and $\tilde{\mathcal{E}}_{k}(\boldsymbol{\mu})$ are monotonically increasing functions with respect to $\mu_{l,k} \quad \forall l, k$. Thus, for $\boldsymbol{\xi}^{\#} \neq \boldsymbol{\xi}^{*}$, we can further reduce $\mu_{l,k} \quad \forall l$ when $E_{k}(\boldsymbol{\xi}^{\#}_{k}) > E_{k}(\boldsymbol{\xi}^{*}_{k})$, and get a new solution $(\boldsymbol{\xi}^{*}, \boldsymbol{\mu}^{*})$ with $\boldsymbol{\mu}^{*} \leq \boldsymbol{\mu}^{\#}$ which can further minimize the objective function Ξ_{tr} . Hence, the optimal solution to $\mathbf{P0}$ can be achieved only when $\boldsymbol{\xi} = \boldsymbol{\xi}^{*}$, which implies that solving $\mathbf{P0}$ is equivalent to solving $\mathbf{P1}$ and $\mathbf{P2}$ in sequence.

In what follows, we discuss methods for solving **P1** and **P2**, respectively.

A. Closed-Form Optimal Solution to P1

Define the following $K \times K$ matrix:

(23)
$$\mathbf{W} = \begin{bmatrix} \mathcal{D}_1 - \Delta_1 \mathcal{U}_1 & -\Delta_1 \mathcal{I}_{12} & \dots & -\Delta_1 \mathcal{I}_{1K} \\ -\Delta_2 \mathcal{I}_{21} & \mathcal{D}_2 - \Delta_2 \mathcal{U}_2 & \dots & -\Delta_2 \mathcal{I}_{2K} \\ \vdots & \vdots & \ddots & \vdots \\ -\Delta_K \mathcal{I}_{K1} & -\Delta_K \mathcal{I}_{K2} & \dots & \mathcal{D}_K - \Delta_K \mathcal{U}_K \end{bmatrix}.$$

We have the following result.

Theorem 3: If **P1** is feasible with $\mathbb{P} \neq \emptyset$, and **W** is invertiable, then the optimal solution $\boldsymbol{\xi}^* = (\xi_1^*, \dots, \xi_K^*)$ of **P1** is given by

$$\boldsymbol{\xi}^* = \boldsymbol{W}^{-1}\boldsymbol{b} \tag{29}$$

where $\boldsymbol{b} = [\Delta_1 \mathcal{N}_1, \Delta_2 \mathcal{N}_2, \dots, \Delta_K \mathcal{N}_K]^T$. In addition, $\boldsymbol{\xi}^*$ simultaneously minimizes the energy consumption for each sensor subject to the target SINR constraints, i.e.,

$$E_k(\xi_k^*) < E_k(\xi_k) \quad \forall k, \text{ with } \boldsymbol{\xi} = (\xi_1, \dots, \xi_K) \in \mathbb{P}.$$
 (30)

Proof: We partition the feasible region \mathbb{P} into

$$\mathbb{P}_{1a} = \{ \boldsymbol{\xi} : \Gamma_1(\boldsymbol{\xi}) > \Delta_1 \text{ and } \Gamma_i(\boldsymbol{\xi}) \geq \Delta_i, j \neq 1 \}$$

and

$$\mathbb{P}_{1b} = \left\{ \boldsymbol{\xi} : \Gamma_1(\boldsymbol{\xi}) = \Delta_1 \text{ and } \Gamma_j(\boldsymbol{\xi}) \ge \Delta_j, \ j \ne 1 \right\}.$$

For any $\bar{\boldsymbol{\xi}} \in \mathbb{P}_{1a}$, there exists a sufficiently small positive value ν and $\bar{\boldsymbol{\xi}} = (\bar{\xi}_1 - \nu, \bar{\xi}_2, \dots, \bar{\xi}_K) \in \mathbb{P}_{1b}$ such that $\sum_{k=1}^K E_k(\tilde{\xi}_k) \leq \sum_{k=1}^K E_k(\bar{\xi}_k)$. Hence, the optimal solution $\boldsymbol{\xi}^* \in \mathbb{P}_{1b}$. Using similar arguments, we can show that $\boldsymbol{\xi}^* \in \mathbb{P}_{kb}$ for any k, where

$$\mathbb{P}_{kb} = \{ \boldsymbol{\xi} : \Gamma_k(\boldsymbol{\xi}) = \Delta_1 \text{ and } \Gamma_i(\boldsymbol{\xi}) \geq \Delta_i, \ j \neq k \}.$$

Thus, $\boldsymbol{\xi}^* \in \mathbb{P}_{1b} \cap \cdots \cap \mathbb{P}_{Kb}$, i.e.,

$$\Gamma_k(\boldsymbol{\xi}^*) = \Delta_k, \quad k = 1, \dots, K. \tag{31}$$

Equation (31) can be rewritten as

$$W\xi^*=b.$$

Next, we prove (30) which is equivalent to

$$\xi_k^* \le \xi_k \quad \forall k, \text{ with } \boldsymbol{\xi} \in \mathbb{P}$$
 (32)

since $E_k(\xi_k)$ is a monotonically increasing function of ξ_k , where \mathbb{P} is the feasibility region defined by (24) and (25). Next, we prove (32) by contradiction. Assume there exists

$$\boldsymbol{\xi}' = (\xi_1', \dots, \xi_K') = (c_1 \xi_1^*, \dots, c_K \xi_K^*) \in \mathbb{P}$$

with some elements $\xi_k' = c_k \xi_k^* < \xi_k^*$, which is equivalent to the existence of some $c_k < 1$. Since (29) and $\xi' \in \mathbb{P}$, we have $\Gamma_k(\xi^*) = \Delta_k$ and $\Gamma_k(\xi') \geq \Delta_k$ for $k = 1, \ldots, K$. Without loss of generality, we assume $c_1 < 1$ and $c_k > 0$, $k \neq 1$. Using $\Gamma_1(\xi^*) = \Delta_1$ and $\Gamma_1(\xi') \geq \Delta_1$, we have

$$\Gamma_{1}(\xi^{*}) = \frac{\mathcal{D}_{1}\xi_{1}^{*}}{\mathcal{U}_{1}\xi_{1}^{*} + \sum_{i \neq 1} \mathcal{I}_{1j}\xi_{i}^{*} + \mathcal{N}_{1}} = \Delta_{1}$$
 (33)

and

$$\Gamma_{1}(\xi') = \frac{\mathcal{D}_{1}c_{1}\xi_{1}^{*}}{\mathcal{U}_{1}c_{1}\xi_{1}^{*} + \sum_{j \neq 1} \mathcal{I}_{1j}\xi_{j}' + \mathcal{N}_{1}} \ge \Delta_{1}.$$
 (34)

Comparing (33) and (34), we obtain

$$\sum_{j \neq 1} \mathcal{I}_{1j} \xi_j' < c_1 \sum_{j \neq 1} \mathcal{I}_{1j} \xi_j^*$$

which implies at least one $c_k < c_1, k = 2, ..., K$. Without loss of generality, we assume $c_2 < c_1$. Using $\Gamma_2(\xi^*) = \Delta_2$ and $\Gamma_2(\xi') \ge \Delta_2$, one can show that at least one $c_k < c_2 < c_1, k = 3, ..., K$. Continuing in this way to satisfy $\Gamma_k(\xi^*) = \Delta_k$ and $\Gamma_k(\xi') \ge \Delta_k$ with k = 1, ..., K - 1, we conclude that

$$c_1 > c_2 >, \dots, > c_K > 0.$$
 (35)

Using $\Gamma_K(\xi^*) = \Delta_K$ and (35), we have

$$\Gamma_K(\boldsymbol{\xi}') = \frac{\mathcal{D}_K c_K \xi_K^*}{\mathcal{U}_K c_K \xi_K^* + \sum_{j \neq 1} \mathcal{I}_{Kj} c_j \xi_j^* + \mathcal{N}_K}$$

$$< \Gamma_K(\boldsymbol{\xi}^*) = \Delta_K$$
(36)

and $\xi' \notin \mathbb{P}$, which contradicts with our assumption. Then, we conclude the proof.

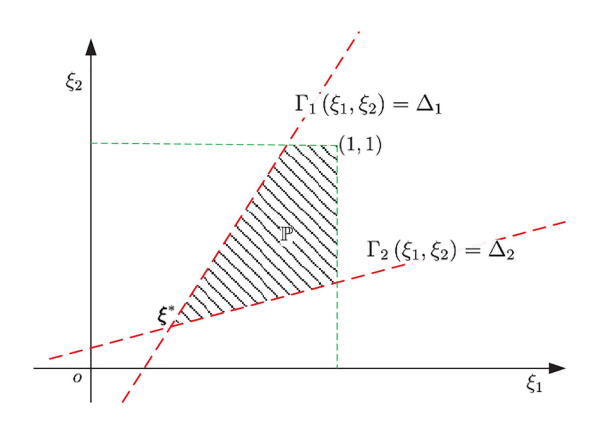


Fig. 3. Feasible region of P1 (shadow area).

To understand Theorem 3, consider the case K = 2. Then, the feasible region \mathbb{P} is

$$\xi_1 \ge \frac{\Delta_1 \mathcal{I}_{12}}{\mathcal{D}_1 - \Delta_1 \mathcal{U}_1} \xi_2 + \frac{\Delta_1}{\mathcal{D}_1 - \Delta_1 \mathcal{U}_1} \mathcal{N}_1$$

and

$$\xi_2 \geq \frac{\Delta_2 \mathcal{I}_{21}}{\mathcal{D}_2 - \Delta_2 \mathcal{U}_2} \xi_1 + \frac{\Delta_2}{\mathcal{D}_2 - \Delta_2 \mathcal{U}_2} \mathcal{N}_2.$$

Thus, \mathbb{P} is the shaded area as shown in Fig. 3. It is straightforward to see that $\boldsymbol{\xi}^*$ is the optimal solution which can simultaneously minimize the energy consumption of both sensors, since the feasible region is a cone.

B. Closed-Form Asymptotically Optimal Solution to P2

According to (21)–(23), P2 can be rewritten as

$$\min_{\mu} Q\left(1 - \frac{\tau}{T}\right) \rho_d N \sum_{l=1}^{L} \sum_{k=1}^{K} \mu_{l,k} \tag{37}$$
s.t.
$$\left[N\left(\sum_{l=1}^{L} \sqrt{\mu_{l,k} \gamma_{l,k}}\right)^2 + \sum_{l=1}^{L} \mu_{l,k} \gamma_{l,k} \right] \ge C_k \quad \forall k \tag{38}$$

where

$$C_k = \frac{E_k(\xi_k) + E_0}{\left(1 - \frac{\tau}{T}\right)Q\zeta\rho_d N}.$$

Then, **P2** is nonconvex due to the nonlinear constraints in (38). Since $\sum_{l=1}^{L} \mu_{l,k} \gamma_{l,k} \leq (\sum_{l=1}^{L} \sqrt{\mu_{l,k} \gamma_{l,k}})^2$, we drop the term $\sum_{l=1}^{L} \mu_{l,k} \gamma_{l,k}$ in (38), to obtain a relaxed problem **P2**′. Note that for massive MIMO, i.e., when N is large, **P2**′ well approximates **P2**. It is not difficult to prove that the optimal solution to **P2**′ is obtained only when

$$N\left(\sum_{l=1}^{L} \sqrt{\mu_{l,k} \gamma_{l,k}}\right)^2 = C_k \quad \forall k.$$
 (39)

Let $\vartheta_{l,k} = \sqrt{\mu_{l,k}}$, then **P2**' becomes

$$\min_{\boldsymbol{\vartheta}} \ Q\left(1 - \frac{\tau}{T}\right) \rho_{d} N \sum_{l=1}^{L} \sum_{k=1}^{K} \vartheta_{l,k}^{2}$$
s.t.
$$\sum_{l=1}^{L} \sqrt{\gamma_{l,k}} \vartheta_{l,k} = \sqrt{C_{k}/N} \quad \forall k$$

$$\vartheta_{l,k} \ge 0 \quad \forall l, k. \tag{40}$$

Algorithm 1 Joint Downlink–Uplink Power Contro Algorithm

- 1: **Input**: The large-scale fading coefficients $\{\beta_{l,k}\}$, the pilot sequence Ψ , and the target SINRs $\{\Delta_k\}$.
- 2: **Step 1**: Calculate the optimal uplink power control coefficients ξ^* according to (29).
- 3: **Step 2**: Calculate the optimal downlink power control coefficients η^* according to (42), (43), and (44).
- 4: Output: ξ^* and η^* .

It is easily seen that P2' can be decomposed into the following K independent minimization problems for k = 1, ..., K:

$$\min_{\vartheta_k} Q\left(1 - \frac{\tau}{T}\right) \rho_d N \sum_{l=1}^L \vartheta_{l,k}^2$$
s.t.
$$\sum_{l=1}^L \sqrt{\gamma_{l,k}} \vartheta_{l,k} = \sqrt{C_k/N}$$

$$\vartheta_{l,k} \ge 0, \quad l = 1, \dots, L. \tag{41}$$

Using the method of the Lagrange multipliers, the closed-form optimal solution to (41) is

$$\vartheta_{l,k}^* = \frac{\sqrt{\gamma_{l,k}C_k/N}}{\sum_{l=1}^L \gamma_{l,k}}, \quad l = 1, \dots, L.$$
 (42)

It is noted that the optimal solution to (40) is a feasible solution to (37), and approaching the optimal solution to (37) as N grows large. After finding ϑ^* , we get $\mu_{l,k}^* = (\vartheta_{l,k}^*)^2$. Furthermore, we use $\mu^* = \lambda \tilde{\eta}$ to find λ and $\tilde{\eta}$. To guarantee the power constraints

$$\sum_{k=1}^{K} \tilde{\eta}_{l,k} \le 1, \quad l = 1, \dots, L$$

we have

$$\sum_{k=1}^K \mu_{l,k}^* \le \lambda, \quad l = 1, \dots, L.$$

Thus, the minimum charging duration is

$$\lambda^* = \max_{l=1,\dots,L} \sum_{k=1}^K \mu_{l,k}^*. \tag{43}$$

Next, we find

$$\tilde{\eta}_{l,k}^* = \frac{\mu_{l,k}^*}{\lambda^*} \text{ and } \eta_{l,k}^* = \frac{\tilde{\eta}_{l,k}^*}{\gamma_{l,k}}.$$
 (44)

The overall algorithm for solving **P0** is summarized in Algorithm 1. In addition, it is easy to extend our proposed algorithm into the nonlinear energy harvesting model [24], [25], since the amount of harvested energy of the kth sensor can be simplified as a monotonically increasing function of \mathcal{E}_k/ζ [26].

V. NUMERICAL RESULTS

In this section, simulation results are provided to corroborate our theoretical analysis and to illustrate the gain due to our proposed system optimization. We consider a large square hall of 50×50 m² with wrapped around to avoid boundary effects. L=144 APs are placed on the ceiling to form a square array with 12 APs in each column and row. K=20 active sensors are randomly distributed in this area. The pilot sequences ψ_k , $k=1,\ldots,K$, are randomly generated and fixed for all simulations. The channel fading coefficients for all scenarios are modeled similar as in [22]. The large-scale fading coefficient $\beta_{l,k}$ is modeled as

$$\beta_{l,k} = \mathcal{L}_{l,k} 10^{\frac{\sigma_{sh}z_{l,k}}{10}}$$

where $\mathcal{L}_{l,k}(\mathrm{dB})$ is the path loss and $10^{[(\sigma_{\mathrm{sh}}z_{lk})/10]}$ is the shadow fading with standard deviation $\sigma_{sh}=8$ dB and $z_{l,k}\sim\mathcal{CN}(0,1)$. Similar to [17], we use the three-slope path-loss model

(41)
$$\mathcal{L}_{l,k} = \begin{cases} -\mathcal{L}_0 - 35 \log_{10}(d_{lk}), & \text{if } d_{lk} > d_1 \\ -\mathcal{L}_0 - 15 \log_{10}(d_1) - 20 \log_{10}(d_{lk}), & \text{if } d_0 < d_{lk} \le d_1 \\ -\mathcal{L}_0 - 15 \log_{10}(d_1) - 20 \log_{10}(d_0), & \text{if } d_{lk} \le d_0 \end{cases}$$
 (45)

with $d_0 = 10$ m, $d_1 = 50$ m, and

$$\mathcal{L}_0 \triangleq 46.3 + 33.9 \log_{10}(f) - 13.82 \log_{10}(h_{\text{AP}}) - (1.1 \log_{10}(f) - 0.7) h_{\text{s}} + (1.56 \log_{10}(f) - 0.8)$$
(46)

where f = 1900 MHz is the carrier frequency, and $h_{AP} = 7$ m and $h_s = 1.65$ m denote the antenna height of APs and sensors, respectively. The transmit power is normalized by the noise power, which is given by

$$\sigma^2 = B \times k_B \times T_0 \times \kappa$$

where $k_B = 1.381 \times 10^{-23}$ J/K is the Boltzmann constant and B is the bandwidth. $T_0 = 290$ K and $\kappa = 9$ dB denote the noise temperature and the noise figure, respectively.

To evaluate the spectrum efficiency, we use the per user throughput defined as

$$R_k = \frac{1 - \tau/T}{(1 + \lambda)} B \log_2(1 + \Gamma_k) \quad \text{b/s.}$$
 (47)

To account for the energy consumption due to pilots and circuits, E_0 in (21) is set as

$$E_0 = (1 + \lambda_0) \frac{\tau}{T} Q \rho_p + (1 + \lambda_0) Q \rho_0$$
 (48)

where $\rho_0 = 0.1$ mW is the circuit power consumption of each sensor, and $\lambda_0 = 50$ is the maximum WPT duration allowed to guarantee the spectrum efficiency. In all examples, we choose the system parameters listed in Table I.

In addition, we fixed the time of data transmission in each period is 1 s, which implies that $Q = 1/T_c = 5$.

We first verify the accuracy of the closed-form expressions $\tilde{\mathcal{E}}_k$ in (18) and Γ_k in (19) for cell-free IoT systems for one realization of large-scale fading $\{\beta_{l,k}\}$. In Fig. 4, the lower bounds $\tilde{\mathcal{E}}_k$, $k=1,\ldots,K$ in (18), are compared with the simulation results obtained by (5) using 500 small-scale fading

	TABLE	I
SIMULAT	TION PAI	RAMETERS

parameter	Meaning	Value
L	Number of APs	144
N	Number of antennas of each AP	10
K	Number of active sensors	20
B	Bandwidth	20 MHz
T_c	Coherence time	0.2 s
T	Number of symbols in each T_c	200
au	Length of pilot	60
P_p	Pilot transmit power	0.2mW
$ ho_p$	Normalized P_p	$\rho_p = \frac{P_p}{\sigma^2}$
P_u	Maximum uplink transmit power	20 mW
$ ho_u$	Normalized P_u	$\rho_u = \frac{P_u}{\sigma^2}$
ζ	Energy conversion efficiency	0.3 [27]
P_d	Maximum downlink transmit power	50 W
$ ho_d$	Normalized P_d	$\rho_d = \frac{P_d}{\sigma^2}$
ξ_k	Uplink power control coefficients	Optimized
$\eta_{l,k}$	Downlink power control coefficients	Optimized
λ	WPT time duration	Optimized

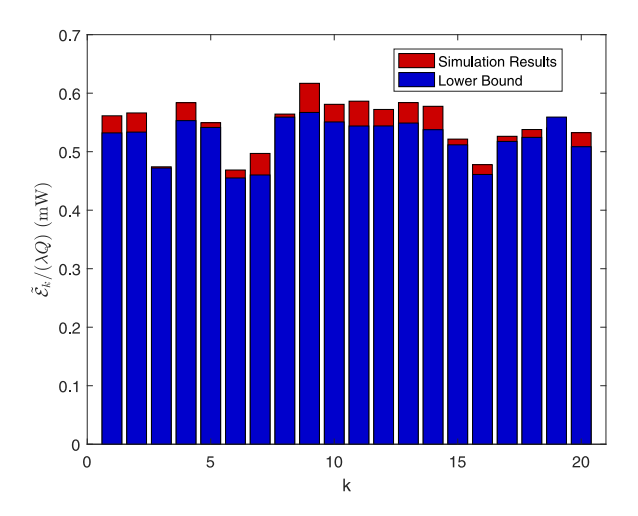


Fig. 4. Tightness of the lower bound $\tilde{\mathcal{E}}_k$ in (18).

channel realizations, under the uniform power control, i.e., $\tilde{\eta}_{l,k} = 1/K \ \forall l, k$. It is seen that the gap between the lower bound $\tilde{\mathcal{E}}_k$ and the simulation result is less than 10%. This is because $\mathbb{E}[|\mathcal{S}_{k1}|^2] \gg \mathbb{E}[|\mathcal{S}_{k2} + \mathcal{S}_{k3}|^2]$ in (17) as N is large. In Fig. 5, the closed-form Γ_k in (19) is compared with the simulation results obtained by (9) using 500 small-scale fading channel realizations with full transmit power, i.e., $\xi_k = 1 \ \forall k$. It is seen that the closed-form expressions match well with the simulation results.

Next, we compare the uplink and downlink performances of three systems which are cell-free IoT, collocated massive MIMO, and small-cell IoT for 200 realizations of large-scale fading $\{\beta_{l,k}\}$. Fig. 6 shows the cumulative distribution function (CDF) of the amount of energy harvested per second, i.e., $\tilde{\mathcal{E}}_k/(\lambda Q)$, for three systems. For cell-free IoT and collocated massive MIMO systems, the uniform power control scheme is adopted. For small-cell IoT, the kth sensor is powered by its associated AP, i.e., $\tilde{\eta}_{l,k} = 1$ if $\delta_{l,k} = 1$. It can be seen that the harvested energy of small-cell IoT is smaller than that of

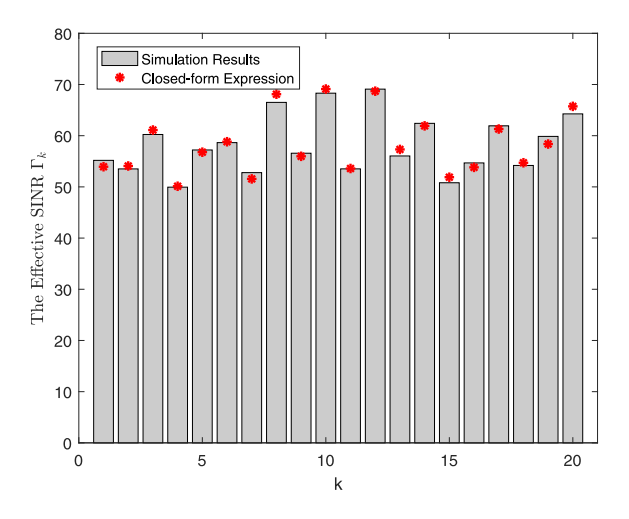


Fig. 5. Accuratey of the SINR expression in (19).

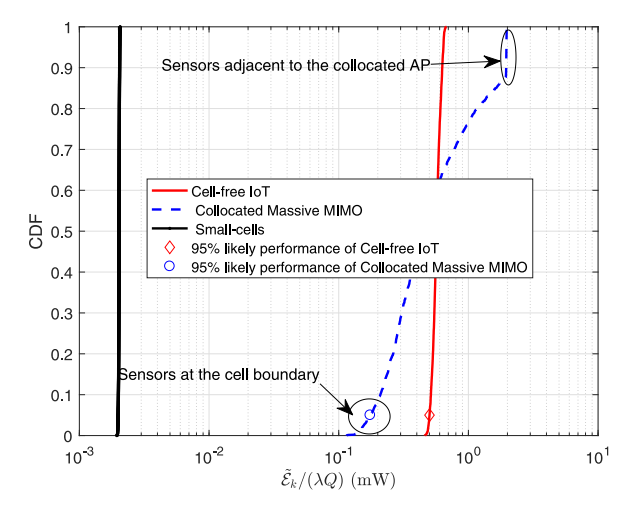


Fig. 6. Downlink performance comparison in terms of $\tilde{\mathcal{E}}_k/(\lambda Q)$ (mW).

the other two systems due to the lower array gain. For collocated massive MIMO, the amount of harvested energy of the cell-boundary sensors is typically small, while that of the sensors adjacent to the AP is very high. Compared with the collocated massive MIMO, the distribution of the harvested energy in cell-free IoT is more concentrated, which results in the substantial improvement of the 95% likely performance. From Fig. 6, it can be seen that the 95% likely performance of cell-free IoT is about five times higher than the collocated massive MIMO. Fig. 7 plots the CDF of the effective SINR for three scenarios with full transmit power, i.e., $\xi_k = 1 \ \forall k$. Similar as the amount of energy harvested, the distribution of effective SINR is more concentrated, and the 95% likely performance is significantly higher than that of the collocated massive MIMO and small-cell IoT. 95% likely performance means the worst performance among 95% of the best sensors which has been widely used in related networks [17], [22]. According to the 95% likely performance, we claim the cellfree network outperforms the collocated massive MIMO and the small-cell IoT, since it can support more networks with higher requirements. It can be seen that about 20% of sensors close to the collocated base station perform better than the cell-free networks. That is, the collocated massive MIMO

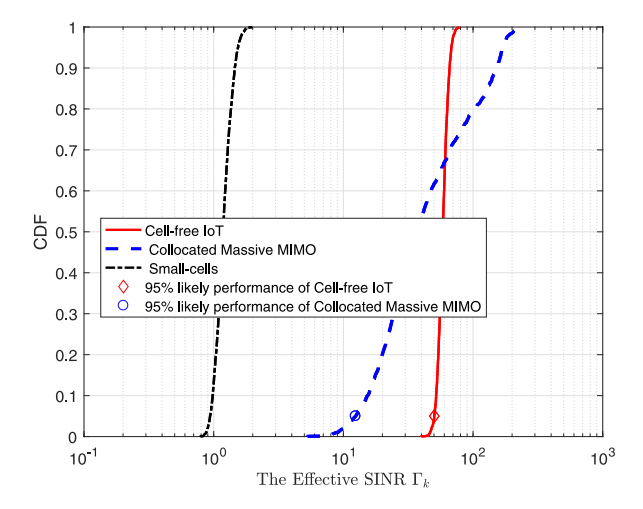


Fig. 7. Uplink performance comparison in terms of SINR.

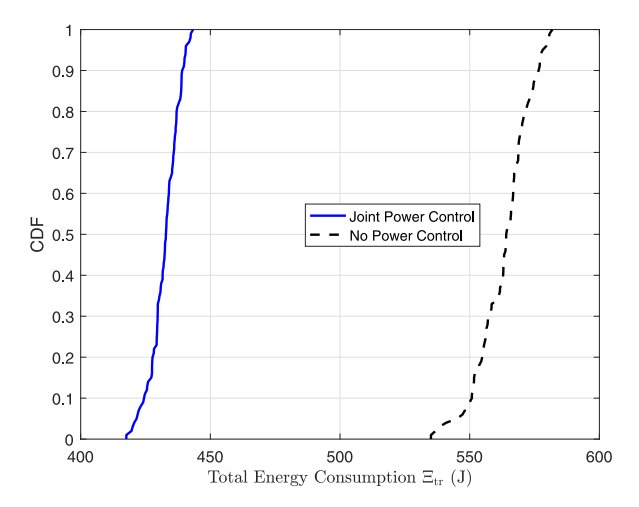


Fig. 8. Performance gain due to joint power control in terms of total energy consumption Ξ_{tr} to support data transmission with given target SINR $\Delta_k = 30, k = 1, \dots, K$, in each period.

outperforms the cell-free network according to the 20% likely performance. However, it is impractical to only support 20% sensors of the whole network.

Finally, the performance of our joint downlink and uplink power control method is investigated. For comparison, we take the no power control scheme with $\xi_k = 1 \ \forall k$ and $\tilde{\eta}_{l,k} = 1/K$ as the benchmark. The result is taken over 200 realizations of large-scale fading $\{\beta_{l,k}\}$. Fig. 8 shows the total energy consumption Ξ_{tr} given in (23) to support data transmission with given target SINR $\Delta_k = 30 \ \forall k$. It can be seen that the total energy consumption Ξ_{tr} can be reduced by about 30% using the joint downlink and uplink power control. On the one hand, the energy consumption of each sensor can be reduced greatly to support the given target SINR using the uplink power control. On the other hand, the total energy consumption can be further reduced through the downlink power control. The CDF of the per user throughput is plotted in Fig. 9. It can be seen that the per user throughput can be improved by 100%, compared with the benchmark. In a word, the energy efficiency can be greatly improved through our joint power control method, in terms of both per user throughput and energy consumption.

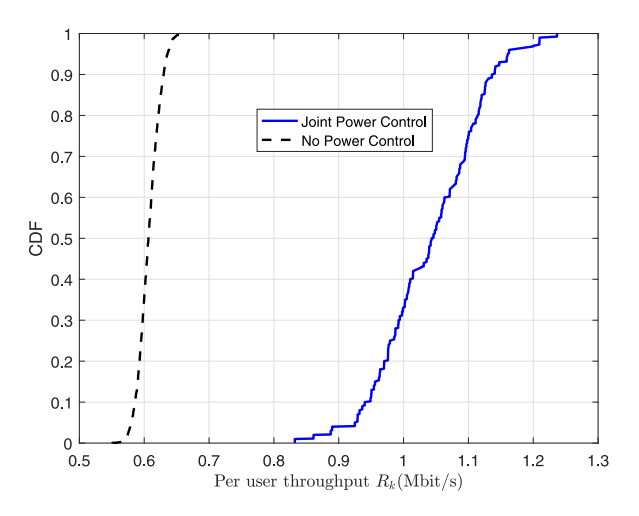


Fig. 9. Performance gain due to joint power control in terms of per user throughput with $\Delta_k=30~\forall k.$

VI. CONCLUSION

In this article, we have proposed a wirelessly powered cell-free IoT system and obtained the closed-form expressions of the downlink and uplink performance metrics, i.e., the amount of harvested energy for downlink, and the SINR for uplink. To minimize the total transmit power consumption under the given SINR constraints, we proposed the joint downlink and uplink power control and provided closed-form solutions. The numerical results indicate that the proposed cell-free massive IoT system significantly outperforms its collocated massive MIMO and small-cell counterparts in terms of both downlink and uplink 95% likely performances. The proposed joint power control further boosts the system performance.

APPENDIX A PROOF OF LEMMA 1

Proof: Using (16), the element of the correlation matrix $\text{cov}[\hat{\mathbf{g}}_{l,k}, \ \hat{\mathbf{g}}_{m,k}]$ in the *n*th row and the \bar{n} th column is

$$\operatorname{cov}\left[\hat{g}_{(l,n),k}, \ \hat{g}_{(m,\bar{n}),k}\right] \\
&= \mathbb{E}\left[\hat{g}_{(l,n),k}\hat{g}_{(m,\bar{n}),k}^{H}\right] - \mathbb{E}\left[\hat{g}_{(l,n),k}\right] \mathbb{E}\left[\hat{g}_{(m,\bar{n}),k}^{H}\right] \\
&= \mathbb{E}\left[\tau \rho_{p} \sum_{i=1}^{K} \sum_{j=1}^{K} g_{(l,n),i}g_{(m,\bar{n}),j} \boldsymbol{a}_{l,k}^{H} \boldsymbol{\varphi}_{i} \boldsymbol{\varphi}_{j}^{H} \boldsymbol{a}_{m,k} + \boldsymbol{a}_{l,k}^{H}\right] \\
&\times \boldsymbol{w}_{(l,n)} \boldsymbol{w}_{(m,\bar{n})}^{H} \boldsymbol{a}_{m,k} + \sqrt{\tau \rho_{p}} \sum_{i=1}^{K} g_{(l,n),i} \boldsymbol{a}_{l,k}^{H} \boldsymbol{\varphi}_{i} \boldsymbol{w}_{(m,\bar{n})}^{H} \boldsymbol{a}_{m,k} \\
&+ \sqrt{\tau \rho_{p}} \sum_{j=1}^{K} g_{(m,\bar{n}),j} \boldsymbol{a}_{m,k}^{H} \boldsymbol{\varphi}_{j} \boldsymbol{w}_{(l,n)}^{H} \boldsymbol{a}_{l,k} \\
&= \operatorname{tr}\left[\mathbb{E}\left(\boldsymbol{w}_{(l,n)} \boldsymbol{w}_{(m,\bar{n})}^{H} \boldsymbol{a}_{m,k} \boldsymbol{a}_{l,k}^{H}\right)\right] \\
&= \operatorname{tr}\left[\mathbb{E}\left(\boldsymbol{w}_{(l,n)} \boldsymbol{w}_{(m,\bar{n})}^{H} \boldsymbol{a}_{m,k} \boldsymbol{a}_{l,k}^{H}\right)\right]$$
(b) O

where step (a) is obtained according to the independence of $g_{(l,n),i}$ and $g_{(m,\bar{n}),j}$, while step (b) is obtained according to the

independence of $w_{(l,n)}$ and $w_{(m,\bar{n})}$. Since each element is zero, the correlation matrix is zero matrix, i.e.,

$$\operatorname{cov}[\hat{\boldsymbol{g}}_{l,k}, \hat{\boldsymbol{g}}_{m,k}] = \mathbf{0}. \tag{49}$$

Using (16), we can obtain

$$\mathbb{E}\left[\hat{g}_{(l,n),k}^{2}, \hat{g}_{(m,\bar{n}),k}^{2}\right] \\
= \mathbb{E}\left[\left(\boldsymbol{a}_{l,k}^{H}\left[\sqrt{\tau\rho_{p}}\sum_{i=1}^{K}g_{(l,n),i}\boldsymbol{\varphi}_{i} + \boldsymbol{w}_{(l,n)}\right]\right)^{2} \\
\times \left(\boldsymbol{a}_{m,k}^{H}\left[\sqrt{\tau\rho_{p}}\sum_{j=1}^{K}g_{(m,\bar{n}),j}\boldsymbol{\varphi}_{j} + \boldsymbol{w}_{(m,\bar{n})}\right]\right)^{2}\right] \\
= \mathbb{E}\left[\left(\tau\rho_{p}\sum_{i=1}^{K}g_{(l,n),i}^{2}\boldsymbol{a}_{l,k}^{H}\boldsymbol{\varphi}_{i}\boldsymbol{a}_{l,k}^{H}\boldsymbol{\varphi}_{i} + \boldsymbol{a}_{l,k}^{H}\boldsymbol{w}_{(l,n)}\boldsymbol{a}_{l,k}^{H}\boldsymbol{w}_{(l,n)}\right) \\
\times \left(\tau\rho_{p}\sum_{j=1}^{K}g_{(m,\bar{n}),j}^{2}\boldsymbol{a}_{m,k}^{H}\boldsymbol{\varphi}_{j}\boldsymbol{a}_{m,k}^{H}\boldsymbol{\varphi}_{j} + \boldsymbol{a}_{m,k}^{H}\boldsymbol{w}_{(m,\bar{n})}\boldsymbol{a}_{m,k}^{H}\boldsymbol{w}_{(m,\bar{n})}\right)\right] \\
= \mathbb{E}\left[\hat{g}_{(l,n),k}^{2}\right]\mathbb{E}\left[\hat{g}_{(m,\bar{n}),k}^{2}\right]. \tag{50}$$

Thus, we have

$$cov \left[\hat{g}_{(l,n),k}^{2}, \ \hat{g}_{(m,\bar{n}),k}^{2} \right] = \mathbb{E} \left[\hat{g}_{(l,n),k}^{2} \hat{g}_{(m,\bar{n}),k}^{2} \right] \\
- \mathbb{E} \left[\hat{g}_{(l,n),k}^{2} \right] \mathbb{E} \left[\hat{g}_{(m,\bar{n}),k}^{2} \right] = 0. (51)$$

By the definition of the ℓ_2 norm, we have

$$\mathbb{E}\Big[\|\hat{\mathbf{g}}_{l,k}\|^{2}\|\hat{\mathbf{g}}_{m,k}\|^{2}\Big] = \mathbb{E}\Big[\left(\sum_{n=1}^{N}\hat{g}_{(l,n),k}^{2}\right)\left(\sum_{\bar{n}=1}^{N}\hat{g}_{(m,\bar{n}),k}^{2}\right)\Big]$$

$$= \sum_{n=1}^{N}\sum_{\bar{n}=1}^{N}\mathbb{E}\Big[\hat{g}_{(l,n),k}^{2}\hat{g}_{(m,\bar{n}),k}^{2}\Big]$$

$$\stackrel{(a)}{=} \sum_{n=1}^{N}\sum_{\bar{n}=1}^{N}\mathbb{E}\Big[\hat{g}_{(l,n),k}^{2}\Big]\mathbb{E}\Big[\hat{g}_{(m,\bar{n}),k}^{2}\Big]$$

$$= \mathbb{E}\left[\sum_{n=1}^{N} \hat{g}_{(l,n),k}^{2}\right] \mathbb{E}\left[\sum_{\bar{n}=1}^{N} \hat{g}_{(m,\bar{n}),k}^{2}\right]$$
$$= \mathbb{E}\left[\left\|\hat{\mathbf{g}}_{l,k}\right\|^{2}\right] \mathbb{E}\left[\left\|\hat{\mathbf{g}}_{m,k}\right\|^{2}\right]$$

where step (a) is obtained by (51). Thus, we have

$$\operatorname{cov} \left[\|\hat{\mathbf{g}}_{l,k}\|^2, \|\hat{\mathbf{g}}_{m,k}\|^2 \right] = 0.$$
 (52)

APPENDIX B PROOF OF THEOREM 1

Proof: First, we compute the power of \mathcal{A}_1 . Since $\hat{\mathbf{g}}_{l,k}$ and $\tilde{\mathbf{g}}_{l,k}$ are independent, we have

$$|\mathcal{A}_1|^2 = \xi_k \rho_u \left| \sum_{l=1}^L \mathbb{E} \left[\hat{\mathbf{g}}_{l,k}^H (\hat{\mathbf{g}}_{l,k} + \tilde{\mathbf{g}}_{l,k}) \right] \right|^2$$
$$= \xi_k \rho_u N^2 \left| \sum_{l=1}^L \gamma_{l,k} \right|^2. \tag{53}$$

Next, we compute the power of A_2 . Since $\hat{\mathbf{g}}_{l,k}$ and $\tilde{\mathbf{g}}_{l,k}$ are independent, and

$$\mathbb{E}\left[\left\|\hat{\boldsymbol{g}}_{l,k}\right\|^{4}\right] = \mathbb{E}\left[\left\|\hat{\boldsymbol{g}}_{l,k}\right\|^{2}\right]^{2} + \mathbb{D}\left[\left\|\hat{\boldsymbol{g}}_{l,k}\right\|^{2}\right] = N(N+1)\gamma_{l,k}^{2}$$

the power of A_2 can be expressed as (54), shown at the bottom of the page, where step (a) is obtained by using Lemma 1.

Then, the power of A_3 can be expressed as

$$\mathbb{E}\left[|\mathcal{A}_3|^2\right] = \sum_{j \neq k} \rho_u \xi_j \mathbb{E}\left[\left|\sum_{l=1}^L \hat{\boldsymbol{g}}_{l,k}^H \boldsymbol{g}_{l,j}\right|^2\right]$$
(55)

where $\mathbb{E}[|\sum_{l=1}^{L} \hat{\mathbf{g}}_{l,k}^{H} \mathbf{g}_{l,j}|^2]$ can be calculated as (56), shown at the top of the next page, with step (a) being obtained by (57), shown at the top of the next page. Substituting (56) into (55), we obtain (58), shown at the top of the next page.

$$\mathbb{E}\Big[|\mathcal{A}_{2}|^{2}\Big] = \rho \xi_{k} \sum_{l=1}^{L} \sum_{m=1}^{L} \mathbb{E}\Big\{\Big(\hat{\mathbf{g}}_{l,k}^{H} \mathbf{g}_{l,k} - \mathbb{E}\Big[\hat{\mathbf{g}}_{l,k}^{H} \mathbf{g}_{l,k}\Big]\Big)\Big(\hat{\mathbf{g}}_{m,k}^{H} \mathbf{g}_{m,k} - \mathbb{E}\Big[\hat{\mathbf{g}}_{m,k}^{H} \mathbf{g}_{m,k}\Big]\Big)^{*}\Big\} \\
= \rho \xi_{k} \sum_{l=1}^{L} \sum_{m=1}^{L} \mathbb{E}\Big[\hat{\mathbf{g}}_{l,k}^{H} (\hat{\mathbf{g}}_{l,k} + \tilde{\mathbf{g}}_{l,k}) \hat{\mathbf{g}}_{m,k}^{H} (\hat{\mathbf{g}}_{m,k}^{*} + \tilde{\mathbf{g}}_{m,k}^{*})\Big] - \rho \xi_{k} N^{2} \sum_{l=1}^{L} \sum_{m=1}^{L} \gamma_{l,k} \gamma_{m,k} \\
= \rho_{u} \xi_{k} \sum_{l=1}^{L} \mathbb{E}\Big[\mathbb{E}\Big[\|\hat{\mathbf{g}}_{l,k}\|^{4}\Big] + \mathbb{E}\Big[\Big|\hat{\mathbf{g}}_{l,k}^{H} \tilde{\mathbf{g}}_{l,k}\Big|^{2}\Big] + \sum_{m \neq l} \mathbb{E}\Big[\|\hat{\mathbf{g}}_{l,k}\|^{2}\|\hat{\mathbf{g}}_{m,k}\|^{2}\Big] + \sum_{m \neq l} \mathbb{E}\Big[\hat{\mathbf{g}}_{l,k}^{H} \tilde{\mathbf{g}}_{l,k} \hat{\mathbf{g}}_{m,k}^{H} \tilde{\mathbf{g}}_{m,k}\Big] \\
+ \sum_{m=1}^{L} \Big\{\mathbb{E}\Big[\|\hat{\mathbf{g}}_{l,k}\|^{2} \hat{\mathbf{g}}_{m,k}^{H} \tilde{\mathbf{g}}_{m,k}\Big] + \mathbb{E}\Big[\|\hat{\mathbf{g}}_{m,k}\|^{2} \hat{\mathbf{g}}_{l,k}^{H} \tilde{\mathbf{g}}_{l,k}\Big]\Big\}\Big] - \rho \xi_{k} N^{2} \sum_{l=1}^{L} \sum_{m=1}^{L} \gamma_{l,k} \gamma_{m,k} \\
\stackrel{(a)}{=} \rho \xi_{k} \sum_{l=1}^{L} \left[N(N+1)\gamma_{l,k}^{2} + N\gamma_{l,k} (\beta_{l,k} - \gamma_{l,k}) + N^{2} \sum_{m \neq l} \gamma_{l,k} \gamma_{m,k}\right] - \rho \xi_{k} N^{2} \sum_{l=1}^{L} \sum_{m=1}^{L} \gamma_{l,k} \gamma_{m,k} \\
= \rho \xi_{k} N \sum_{l=1}^{L} \gamma_{l,k} \beta_{l,k} \tag{54}$$

$$\mathbb{E}\left[\left|\sum_{l=1}^{L} \hat{\mathbf{g}}_{l,k}^{H} \mathbf{g}_{l,j}\right|^{2}\right] = \mathbb{E}\left[\left|\sum_{l=1}^{L} \sum_{n=1}^{N} g_{(l,n),j} \hat{\mathbf{g}}_{(l,n),k}^{*}\right|^{2}\right] \\
= \mathbb{E}\left[\left|\sum_{l=1}^{L} \sum_{n=1}^{N} g_{(l,n),j} \left(\mathbf{a}_{l,k}^{H} \left[\sqrt{\tau \rho_{p}} \sum_{i=1}^{K} g_{(l,n),i} \boldsymbol{\varphi}_{i} + \mathbf{w}_{(l,n)}\right]\right)^{*}\right|^{2}\right] \\
= \mathbb{E}\left[\left|\sqrt{\tau \rho_{p}} \sum_{l=1}^{L} \sum_{n=1}^{N} g_{(l,n),j} \sum_{i=1}^{K} g_{(l,n),i}^{*} \mathbf{a}_{l,k}^{T} \boldsymbol{\varphi}_{i}^{*} + \sum_{l=1}^{L} \sum_{n=1}^{N} g_{(l,n),j} \mathbf{a}_{l,k}^{T} \mathbf{w}_{(l,n)}^{*}\right|^{2}\right] \\
= \mathbb{E}\left[\left|\sum_{l=1}^{L} \sum_{n=1}^{N} g_{(l,n),j} \mathbf{a}_{l,k}^{T} \mathbf{w}_{(l,n)}^{*}\right|^{2} + \tau \rho_{p} \mathbb{E}\left[\left|\sum_{l=1}^{L} \sum_{i=1}^{K} g_{l,i}^{H} \mathbf{g}_{l,j} \mathbf{a}_{l,k}^{T} \boldsymbol{\varphi}_{i}^{*}\right|^{2}\right] \\
= \sum_{l=1}^{L} \beta_{l,j} N \|\mathbf{a}_{l,k}\|_{2}^{2} + \tau \rho_{p} \mathbb{E}\left[\sum_{l=1}^{L} \sum_{i=1}^{K} \sum_{l=1}^{L} \sum_{i=1}^{K} \mathbf{g}_{l,i}^{H} \mathbf{g}_{l,j} \mathbf{g}_{\bar{l},i}^{H} \mathbf{g}_{\bar{l},j} \mathbf{a}_{l,k}^{T} \boldsymbol{\varphi}_{i}^{*} \mathbf{a}_{\bar{l},k}^{T} \boldsymbol{\varphi}_{i}^{*}\right] \\
\stackrel{(a)}{=} \sum_{l=1}^{L} \beta_{l,j} N \|\mathbf{a}_{l,k}\|_{2}^{2} + \tau \rho_{p} \left(N^{2} \left|\sum_{l=1}^{L} \beta_{l,j} \boldsymbol{\psi}_{j}^{H} \mathbf{a}_{l,k}\right|^{2} + \sum_{l=1}^{L} \sum_{i=1}^{K} N \beta_{l,j} \beta_{l,i} |\boldsymbol{\psi}_{i}^{H} \mathbf{a}_{l,k}|^{2}\right)$$
(56)

$$\mathbb{E}\left[\mathbf{g}_{l,i}^{H}\mathbf{g}_{l,j}\mathbf{g}_{\bar{l},\bar{l}}^{H}\mathbf{g}_{\bar{l},j}\right] = \begin{cases} \mathbb{E}\left[\left\|\mathbf{g}_{l,j}\right\|^{4}\right] = N(N+1)\beta_{l,j}^{2}, & \bar{l} = l, \ \bar{i} = i = j \\ \mathbb{E}\left[\left\|\mathbf{g}_{l,j}^{H}\mathbf{g}_{l,i}\right\|^{2}\right] = N\beta_{l,j}\beta_{l,i}, & \bar{l} = l, \ \bar{i} = i \neq j \\ \mathbb{E}\left[\left\|\mathbf{g}_{l,j}\right\|^{2}\left\|\mathbf{g}_{\bar{l},j}\right\|^{2}\right] = N^{2}\beta_{l,j}\beta_{\bar{l},j}, \ \bar{l} \neq l, \ \bar{i} = i = j \\ 0, & \text{otherwise} \end{cases}$$

$$(57)$$

$$\mathbb{E}\Big[|\mathcal{A}_{3}|^{2}\Big] = \sum_{j \neq k} \rho_{u} N \xi_{j} \left[\sum_{l=1}^{L} \beta_{l,j} \|\boldsymbol{a}_{l,k}\|^{2} + \tau \rho_{p} \left(N \left| \sum_{l=1}^{L} \beta_{l,j} \boldsymbol{\psi}_{j}^{H} \boldsymbol{a}_{l,k} \right|^{2} + \sum_{l=1}^{L} \sum_{i=1}^{K} \beta_{l,j} \beta_{l,i} |\boldsymbol{\psi}_{i}^{H} \boldsymbol{a}_{l,k}|^{2} \right) \right]$$
(58)

Finally, we compute the power of A_4 . Due to the independence of $\hat{\mathbf{g}}_{l,k}$ and $\tilde{\mathbf{g}}_{l,k}$, we have

$$\mathbb{E}\left[|\mathcal{A}_4|^2\right] = \mathbb{E}\left[\left|\sum_{l=1}^L \hat{\boldsymbol{g}}_{l,k}^H \boldsymbol{n}_l\right|^2\right] = N \sum_{l=1}^L \gamma_{l,k}.$$
 (59)

Plugging (53), (54), (58), and (59) into (9), we obtain (19).

REFERENCES

- A. Al-Fuqaha, M. Guizani, M. Mohammadi, M. Aledhari, and M. Ayyash, "Internet of Things: A survey on enabling technologies, protocols, and applications," *IEEE Commun. Surveys Tuts.*, vol. 17, no. 4, pp. 2347–2376, 4th Quart., 2015.
- [2] L. D. Xu, W. He, and S. Li, "Internet of Things in industries: A survey," IEEE Trans. Ind. Informat., vol. 10, no. 4, pp. 2233–2243, Nov. 2014.
- [3] Z. Chu, F. Zhou, Z. Zhu, R. Q. Hu, and P. Xiao, "Wireless powered sensor networks for Internet of Things: Maximum throughput and optimal power allocation," *IEEE Internet Things J.*, vol. 5, no. 1, pp. 310–321, Feb. 2018.
- [4] S. H. Chae, C. Jeong, and S. H. Lim, "Simultaneous wireless information and power transfer for Internet of Things sensor networks," *IEEE Internet Things J.*, vol. 5, no. 4, pp. 2829–2843, Aug. 2018.
- [5] D. S. Gurjar, H. H. Nguyen, and H. D. Tuan, "Wireless information and power transfer for IoT applications in overlay cognitive radio networks," *IEEE Internet Things J.*, vol. 6, no. 2, pp. 3257–3270, Apr. 2019.

- [6] Y. Alsaba, S. K. A. Rahim, and C. Y. Leow, "Beamforming in wireless energy harvesting communications systems: A survey," *IEEE Commun. Surveys Tuts.*, vol. 20, no. 2, pp. 1329–1360, 2nd Quart., 2018.
- [7] T. D. P. Perera, D. N. K. Jayakody, S. K. Sharma, S. Chatzinotas, and J. Li, "Simultaneous wireless information and power transfer (SWIPT): Recent advances and future challenges," *IEEE Commun. Surveys Tuts.*, vol. 20, no. 1, pp. 264–302, 1st Quart., 2018.
- [8] X. Lu, P. Wang, D. Niyato, D. I. Kim, and Z. Han, "Wireless networks with RF energy harvesting: A contemporary survey," *IEEE Commun. Surveys Tuts.*, vol. 17, no. 2, pp. 757–789, 2nd Quart., 2015.
- [9] J. Huang, C. Xing, and C. Wang, "Simultaneous wireless information and power transfer: Technologies, applications, and research challenges," *IEEE Commun. Mag.*, vol. 55, no. 11, pp. 26–32, Nov. 2017.
- [10] T. A. Khan, A. Yazdan, and R. W. Heath, "Optimization of power transfer efficiency and energy efficiency for wireless-powered systems with massive MIMO," *IEEE Trans. Wireless Commun.*, vol. 17, no. 11, pp. 7159–7172, Nov. 2018.
- [11] X. Wu, W. Xu, X. Dong, H. Zhang, and X. You, "Asymptotically optimal power allocation for massive MIMO wireless powered communications," *IEEE Wireless Commun. Lett.*, vol. 5, no. 1, pp. 100–103, Feb. 2016.
- [12] X. Wang, J. Liu, and C. Zhai, "Wireless power transfer-based multipair two-way relaying with massive antennas," *IEEE Trans. Wireless Commun.*, vol. 16, no. 11, pp. 7672–7684, Nov. 2017.
- [13] G. Amarasuriya, E. G. Larsson, and H. V. Poor, "Wireless information and power transfer in multiway massive MIMO relay networks," *IEEE Trans. Wireless Commun.*, vol. 15, no. 6, pp. 3837–3855, Jun. 2016.
- [14] S. Lee and R. Zhang, "Distributed wireless power transfer with energy feedback," *IEEE Trans. Signal Process.*, vol. 65, no. 7, pp. 1685–1699, Apr. 2017.

- [15] W. Kim and W. Yoon, "Energy efficiency maximisation for WPCN with distributed massive MIMO system," *Electron. Lett.*, vol. 52, no. 19, pp. 1642–1644, Sep. 2016.
- [16] Z. Zhu, S. Huang, Z. Chu, F. Zhou, D. Zhang, and I. Lee, "Robust designs of beamforming and power splitting for distributed antenna systems with wireless energy harvesting," *IEEE Syst. J.*, vol. 13, no. 1, pp. 30–41, Mar. 2019.
- [17] H. Q. Ngo, A. Ashikhmin, H. Yang, E. G. Larsson, and T. L. Marzetta, "Cell-free massive MIMO versus small cells," *IEEE Trans. Wireless Commun.*, vol. 16, no. 3, pp. 1834–1850, Mar. 2017.
- [18] E. Nayebi, A. Ashikhmin, T. L. Marzetta, H. Yang, and B. D. Rao, "Precoding and power optimization in cell-free massive MIMO systems," *IEEE Trans. Wireless Commun.*, vol. 16, no. 7, pp. 4445–4459, Jul. 2017.
- [19] S. Buzzi and C. D'Andrea, "Cell-free massive MIMO: User-centric approach," *IEEE Wireless Commun. Lett.*, vol. 6, no. 6, pp. 706–709, Dec. 2017.
- [20] H. Q. Ngo, L. Tran, T. Q. Duong, M. Matthaiou, and E. G. Larsson, "On the total energy efficiency of cell-free massive MIMO," *IEEE Trans. Green Commun. Netw.*, vol. 2, no. 1, pp. 25–39, Mar. 2018.
- [21] L. D. Nguyen, T. Q. Duong, H. Q. Ngo, and K. Tourki, "Energy efficiency in cell-free massive MIMO with zero-forcing precoding design," *IEEE Commun. Lett.*, vol. 21, no. 8, pp. 1871–1874, Aug. 2017.
- IEEE Commun. Lett., vol. 21, no. 8, pp. 1871–1874, Aug. 2017.
 [22] S. Rao, A. Ashikhmin, and H. Yang, "Internet of Things based on cell-free massive MIMO," in Proc. 53rd Asilomar Conf. Signals Syst. Comput., Pacific Grove, CA, USA, 2019, pp. 1946–1950.
- [23] B. Hassibi and B. M. Hochwald "How much training is needed in multiple-antenna wireless links?" *IEEE Trans. Inf. Theory*, vol. 49, no. 4, pp. 951–963, Apr. 2003.
- [24] X. Zhang, Y. Wang, F. Zhou, N. Al-Dhahir, and X. Deng, "Robust resource allocation for MISO cognitive radio networks under two practical non-linear energy harvesting models," *IEEE Commun. Lett.*, vol. 22, no. 9, pp. 1874–1877, Sep. 2018.
- [25] H. Sun, F. Zhou, R. Q. Hu, and L. Hanzo, "Robust beamforming design in a NOMA cognitive radio network relying on SWIPT," *IEEE J. Sel. Areas Commun.*, vol. 37, no. 1, pp. 142–155, Jan. 2019.
- [26] S. Wang, M. Xia, K. Huang, and Y. Wu, "Wirelessly powered two-way communication with nonlinear energy harvesting model: Rate regions under fixed and mobile relay," *IEEE Trans. Wireless Commun.*, vol. 16, no. 12, pp. 8190–8204, Dec. 2017.
- [27] Z. Zhu, Z. Chu, F. Zhou, H. Niu, Z. Wang, and I. Lee, "Secure beamforming designs for secrecy MIMO SWIPT systems," *IEEE Wireless Commun. Lett.*, vol. 7, no. 3, pp. 424–427, Jun. 2018.



Xinhua Wang (Member, IEEE) received the Ph.D. degree in communication and information system from Shandong University, Jinan, China, in 2016.

In June 2016, he joined the College of Electrical Engineering, Qingdao University, Qingdao, China, as a Lecturer. His research interests include massive MIMO, cell-free massive MIMO, compressed sensing, and random matrix theory.



Alexei Ashikhmin (Fellow, IEEE) received the Ph.D. degree in electrical engineering from the Institute of Information Transmission Problems, Russian Academy of Science, Moscow, Russia, in 1994.

He is a Distinguished Member of Technical Staff with the Communications and Statistical Sciences Research Department, Nokia Bell Labs, Murray Hill, NJ, USA. He is also an Adjunct Professor with Columbia University, New York, NY, USA, where he teaches courses on quantum computing and error

correction, digital communications, and error correcting codes. His research interests include communications theory, massive MIMO systems, theory of error correcting codes and its modern applications, as well as classical and quantum information theory.

Dr. Ashikhmin was a recipient of the 2017 SPS Donald G. Fink Overview Paper Award for the article An Overview of Massive MIMO: Benefits and Challenges published in the IEEE JOURNAL OF SELECTED TOPICS IN SIGNAL PROCESSING. In 2014, he received the Thomas Edison Patent Award in the Telecommunications for a Patent on Massive MIMO System with Decentralized Service Antennas. In 2004, he received the IEEE Communications Society Stephen O. Rice Prize for the best paper published in the IEEE TRANSACTIONS ON COMMUNICATIONS. In 2002, 2010, and 2011, he was a recipient of the Bell Laboratories President Award for breakthrough research in wired and wireless communication projects.



Xiaodong Wang (Fellow, IEEE) received the Ph.D. degree in electrical engineering from Princeton University, Princeton, NJ, USA, in 1998.

He is a Professor of electrical engineering with Columbia University, New York, NY, USA. His research interests fall in the general areas of computing, signal processing, and communications, and has published extensively in these areas. Among his publications is a book titled *Wireless Communication Systems: Advanced Techniques for Signal Reception* (Prentice Hall in 2003). His current research interests

include wireless communications, statistical signal processing, and genomic signal processing.

Dr. Wang received the 1999 NSF CAREER Award, the 2001 IEEE Communications Society and Information Theory Society Joint Paper Award, and the 2011 IEEE Communication Society Award for Outstanding Paper on New Communication Topics. He has served as an Associate Editor for the IEEE TRANSACTIONS ON COMMUNICATIONS, the IEEE TRANSACTIONS ON WIRELESS COMMUNICATIONS, the IEEE TRANSACTIONS ON SIGNAL PROCESSING, and the IEEE TRANSACTIONS ON INFORMATION THEORY. He is listed as an ISI Highly Cited Author.